

UC San Diego

UC San Diego Electronic Theses and Dissertations

Title

Non-GCA Modeling of Near Threshold IV Characteristics of DG MOSFETs

Permalink

<https://escholarship.org/uc/item/4j36q4hs>

Author

Ren, Zhongjie

Publication Date

2020

Peer reviewed|Thesis/dissertation

UNIVERSITY OF CALIFORNIA SAN DIEGO

Non-GCA Modeling of Near Threshold IV Characteristics of DG MOSFETs

A Thesis submitted in partial satisfaction of the requirements for the
degree Master of Science

in

Electrical and Computer Engineering

by

Zhongjie Ren

Committee in charge:

Professor Yuan Taur, Chair
Professor Shadi A. Dayeh
Professor Tse Nga Ng

2020

Copyright ©

Zhongjie Ren, 2020

All rights reserved.

The Thesis of Zhongjie Ren is approved, and it is acceptable in quality and form for publication on microfilm and electronically:

Chair

University of California San Diego

2020

TABLE OF CONTENTS

Signature Page.....	iii
Table of Contents.....	iv
List of Figures	v
Acknowledgements.....	vii
Abstract of the Thesis	xi
Introduction.....	1
Chapter 1 Non-GCA Model in the Velocity Saturation Region	2
Chapter 2 Limitations of Linear $Q_i(V)$ Model in the Near Threshold Region.....	6
Chapter 3 Construction of Piecewise $Q_i(V)$	10
Chapter 4 Non-GCA Model with Piecewise $Q_i(V)$ for the Near-Threshold Region.....	16
Conclusion	25
References.....	26

LIST OF FIGURES

Figure 1 Schematic structure of DG MOSFET involved in this work. $L = 50\text{nm}$, $t_{si} = 4\text{nm}$, $t_i = 2\text{nm}$, $\epsilon_{si}=\epsilon_i=11.8\epsilon_0$. The gate work function is such that $V_t = 0.33\text{V}$	3
Figure 2 I_{ds} - V_{ds} characteristics for above threshold region generated by linear $Q_i(V)$ model [Eq. (3)] compared with TCAD for (a) $n = 1$ and (b) $n = 2$ velocity saturation cases. $\mu_0=200\text{cm}^2/\text{V}\cdot\text{s}$ and $v_{\text{sat}} = 10^7\text{cm/s}$	5
Figure 3 I_{ds} - V_{ds} characteristics for near threshold region generated by Non-GCA model with linear $Q_i(V)$ [Eq.(3)] compared with TCAD for (a) $n = 1$ and (b) $n = 2$ velocity saturation cases	7
Figure 4 Comparison of $Q_i(V)$ extracted from TCAD and linear model [Eq.(3)] for (a) $V_{gs}=0.6\text{V}$ (above threshold region), (b) $V_{gs}=0.35\text{V}$ (near threshold region)	9
Figure 5 Comparison of $Q_i(V)$ extracted from TCAD , linear model [Eq.(3)] and Eq. (9) for $V_{gs}=0.35\text{V}$ (near threshold region)	12
Figure 6 Comparison of $Q_i(V)$ extracted from TCAD and turning points (TP-1 & TP-2) for $V_{gs}=0.35/0.4\text{V}$ calculated by facilitating $G(V)$	14
Figure 7 Comparison of $Q_i(V)$ extracted from TCAD, linear model [Eq.(3)] , Eq. (19) and piecewise model [Eqs.(20) and (21)] for $V_{gs}=0.35\text{V}$	16
Figure 8 (a) $V(y)$ and (b) $Q_i(y)$ in the channel extracted from TCAD, non-GCA model with linear $Q_i(V)$ [Eq.(3)] and piecewise $Q_i(V)$ [Eqs.(20) and (21)] for $V_{gs}=0.35\text{V}$ and $V_{ds}=1.2\text{V}$	18
Figure 9 (a) $V(y)$ and (b) $Q_i(y)$ in the channel extracted from TCAD, non-GCA model with linear $Q_i(V)$ [Eq.(3)] and piecewise $Q_i(V)$ [Eqs.(20) and (21)] for $V_{gs}=0.4\text{V}$ and $V_{ds}=1.2\text{V}$	19
Figure 10 I_{ds} - V_{ds} characteristics ($n = 1$ velocity saturation case) for the near threshold region generated by non-GCA model with piecewise $Q_i(V)$ [Eqs.(20) and (21)] compared with TCAD for (a) $n = 1$ and (b) $n = 2$ velocity saturation cases.	21
Figure 11 Comparison of $Q_i(y)$ in the channel between the non-GCA model with piecewise $Q_i(V)$ [Eqs.(20) and (21)] and TCAD.	22
Figure 12 I_{ds} - V_{gs} characteristics generated by the non-GCA model with linear $Q_i(V)$ [Eq. (2)] and with piecewise $Q_i(V)$ [Eqs.(20) and (21)] compared to TCAD for (a) $n = 1$ and (b) $n = 2$ velocity saturation models. $V_t \sim 0.33\text{V}$ in this case.	23

Figure 13 I_{ds} - V_{ds} characteristics for the above threshold region generated by non-GCA model with piecewise $Q_i(V)$ [Eqs.(20) and (21)] compared with TCAD for (a) $n = 1$ and (b) $n = 2$ velocity saturation cases.....24

ACKNOWLEDGEMENTS

I would like to acknowledge Professor Yuan Taur for his support as the chair of my committee. I really appreciated his guidance and suggestions which profoundly improve this thesis. Apart from his support in academia, his dedication and achievement in science inspired me in pursuing my own career. I will always remember to ‘make things happen’ instead of ‘wait things happen’, as he taught me when I entered his group. Besides, I would like to thank the rest of my thesis committee: Prof. Shadi Dayeh and Prof. Tse Nga Ng who provided insightful suggestions and discussion on my thesis defense.

I thank my teammates in Prof. Taur’s group: Chuyang Hong, Mei-Hua Su and Jianing Zhang for helping me on my research work and simulation tools. Special thanks to Dr. Woojin Choi for tutoring me on the Slivaco TCAD. I would like to express my appreciation to my friends who came in my master’s life: Yong Zhang, Ben Qiu, Xinyu Chen, Clara Tong, Mingyang Liu, Huabin Yu, Danhao Wang, Chong Xing, Zhongling Liu, Zhiqiang Sun, Zhengqiang Ma, Yi Peng, Zixi Wang and others who supported and encouraged me. Sincere thanks to Ride Bu for her support and friendship.

I would also like to thank Prof. Haiding Sun, Prof. Xiaohang Li, Prof. Yuping Zeng and Prof. Qizhen Sun for enlightening the first glance of research back in my college. Last but not the least, I would like to thank my parents for unconditional support throughout my life.

Part of the data and graphs in this thesis is a reprint of the material as it is in
Solid-State Electronics, vol. 166, Art. no. 107766, Ren, Zhongjie, Taur, Yuan.

The thesis author was the primary investigator and author of this paper.

ABSTRACT OF THE THESIS

Non-GCA Modeling of Near Threshold IV Characteristics of
DG MOSFETs

by

Zhongjie Ren

Master of Science in Electrical and Computer Engineering

University of California San Diego, 2020

Professor Yuan Taur, Chair

It is well known that the velocity saturation behavior is not negligible in the

shorter channel length and the gradual channel approximation (GCA) fails to generate reasonable I-V characteristics of MOSFETs for both $n = 1$ and $n = 2$ models. Therefore, the non-GCA model has been developed to solve this issue by adding the ΔQ (Source-Drain induced part for mobile charges) term which is absent in the conventional GCA models and exhibits an excellent performance for above threshold region ($V_{gs}-V_t>0.27V$) modeling. However, the near threshold modeling ($V_{gs}-V_t<0.1V$) is not ideal in the previous non-GCA model with linear $Q_i(V)$ when compared with TCAD simulations owing to the failure of matching the $Q_i(V)$ (Gate induced part for mobile charges) profile in that region. In this work, a more rigorous non-GCA model with piecewise $Q_i(V)$ which can successfully approach I-V behaviors of DG MOSFETs in the near threshold region for $n = 1$ and $n = 2$ has been proposed by extending the continuous, analytical GCA model of $Q_i(V)$ to obtain negative values. In addition, relative favorable above threshold I-V characteristics can be calculated by utilizing the proposed non-GCA model as well.

Introduction

The double gate (DG) MOSFET is usually considered as the ideal physical model of FinFETs which are commonly utilized in the current CMOS manufacturing. So far, compact constant mobility models for DG MOSFET have been extensively investigated in the past decades [1-4]. However, when the channel length keeps shrinking, it is nonphysical to assume constant mobility in the device which will significantly overestimate the source-drain current value of MOSFETs [5]. Consequently, the velocity saturation behavior should be taken into account and specific models working in this regime requires further investigation.

In the constant mobility situation, the gradual channel approximation (GCA) assumes that mobile charges in the channel are mainly determined by the longitudinal gradient part of 2-D Poisson's equation, thus it is reasonable to ignore the contribution of the lateral gradient part. In fact, this assumption works well in the long channel DG MOSFET but is no longer valid in devices with smaller channel length. Most GCA models will stop at the saturation point when I_{ds} peaks, thereby failing to predict the I_{ds} values in the velocity saturation region [6]. Therefore, additional modification should be carried out in order to compensate the lack of lateral gradient in the GCA model. Recently, new analytical model has been proposed to extend I-V characteristics into the velocity saturation region for both $n = 1$ and $n = 2$ models [7]. Moreover,

promising I_{ds} - V_{ds} curves which are well fitted with TCAD simulation [8] results have been observed. However, only the above threshold region ($V_{gs}-V_t>0.2\text{V}$) was investigated in that study while modeling of DG MOSFETs in the near threshold region ($V_{gs}-V_t<0.1\text{V}$) which is important for the design of low-power analog circuits remains blank. Apparently, further efforts should be devoted to the I-V characteristics modeling in this region.

In this work, the previous reported non-GCA model with linear $Q_i(V)$ has been tested for the near threshold performance and it turns out to generate separated I_{ds} - V_{ds} curves compared to TCAD data for $n = 1$ and $n = 2$ situations. Thus, a new model for velocity saturation has been proposed by using a piecewise $Q_i(V)$ to achieve the generation of continuous closed I_{ds} - V_{ds} curves with TCAD simulations in the near threshold region. Furthermore, the above threshold I-V characteristics in the proposed model which excellently match TCAD data can be obtained, illustrating the universality of this model in both near and above threshold regions.

Chapter 1: Non-GCA Model in the Velocity Saturation Region

The schematic cross-section of the DG MOSFET utilized in this work is shown in Fig.1. Based on the velocity saturation model, the source-drain

current (I_{ds}) is determined by the following equations for $n = 1$, $n = 2$,

respectively:

$$I_{ds} = \mu W Q_t \frac{dV}{dy} = \frac{\mu_0 W Q_t}{1 + (\mu_0/v_{sat})(dV/dy)} \frac{dV}{dy} (n=1) \quad (1)$$

$$I_{ds} = \mu W Q_t \frac{dV}{dy} = \frac{\mu_0 W Q_t}{\sqrt{1 + (\mu_0/v_{sat})^2 (dV/dy)^2}} \frac{dV}{dy} (n=2) \quad (2)$$

where μ_0 is the low-field mobility, v_{sat} is the saturation velocity, W is the width of the device, Q_t is the total mobile charge per unit area, and V is the electron quasi-Fermi potential at the position y in the channel.

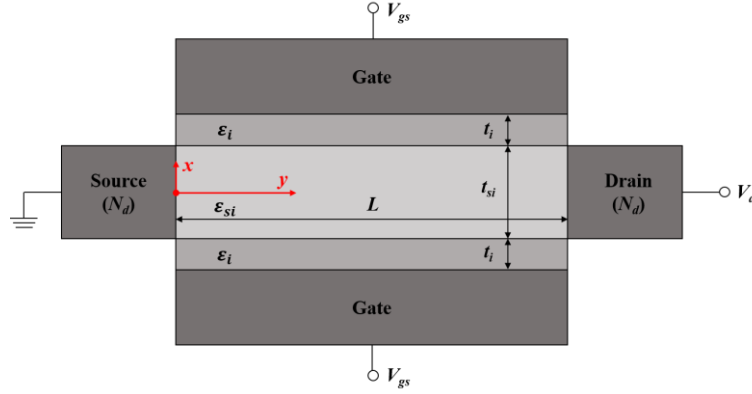


Figure 1 Schematic structure of DG MOSFET involved in this work. $L =$

50nm , $t_{si} = 4\text{nm}$, $t_i = 2\text{nm}$, $\epsilon_{si} = \epsilon_i = 11.8\epsilon_0$. The gate work function is such that V_t

$= 0.33\text{V}$

Recently, a non-GCA model with linear $Q_i(V)$ has successfully reproduced above threshold I-V characteristics of DG MOSFETs in the velocity saturation region [6].

$$Q_t = Q_i + \Delta Q_{non-GCA} = 2C_{inv} (V_{gs} - V_t - V) + \epsilon_{si} t_{si} \frac{d^2V}{dy^2} \quad (3)$$

where Q_i is the part which attributes to the longitudinal gradient, d^2V/dx^2 ,

while $\Delta Q_{\text{non-GCA}}$ is another part which results from the lateral gradient (non-GCA part), d^2V/dy^2 , C_{inv} is the inversion layer capacitance per unit area and V_t is the threshold voltage. The non-GCA part is crucial for velocity saturation modeling since it permits the model to extend to the saturation points, which can not be achieved in any GCA model. By applying this non-GCA model in calculating mobile charge in the channel, we can obtain the following equations for $n = 1$ velocity saturation model

$$\frac{I_{ds}}{\mu_0 W} y + \frac{I_{ds}}{v_{sat} W} V = 2C_{\text{inv}} \left[(V_{gs} - V_t) V - \frac{V^2}{2} \right] + \frac{\epsilon_{si} t_{si}}{2} \left[\left(\frac{dV}{dy} \right)^2 - E_0^2 \right] \quad (4)$$

$$E_0 = \left(dV/dy \right) \Big|_{y=0} = \frac{I_{ds}}{\mu_0 W Q_i(V=0) - (\mu_0/v_{sat}) I_{ds}} \quad (5)$$

For the $n = 2$ velocity saturation model, the equations switch to the following format

$$I_{ds}^2 \left[1 + \left(\frac{\mu_0}{v_{sat}} \right)^2 g \right] = W^2 \mu_0^2 g \left[2C_{\text{inv}} (V_{gs} - V_t - V) + \frac{\epsilon_{si} t_{si}}{2} \frac{dg}{dV} \right]^2 \quad (6)$$

$$g(V) = \left(\frac{dV}{dy} \right)^2 \quad (7)$$

The detailed integration process for Eqs. (4) and (5) can be found in Ref.[6]. For a given I_{ds} , Eq. (4) can be solved to obtain all the way to $V_{ds}=V(y=L)$, thereby buliding the I-V characterisitics for the $n = 1$ velocity saturation model of Non-GCA model with linear $Q_i(V)$. For the $n = 2$ situation, Eq. (6) can be obtained by integrating $g-1/2$ through the channel and therefore approaches the solution of I_{ds} - V_{ds} . As shown in Figs. 2(a) and 2(b), the I-V curves for $n = 1$ and $n = 2$ generated by Non-GCA model with linear $Q_i(V)$ are

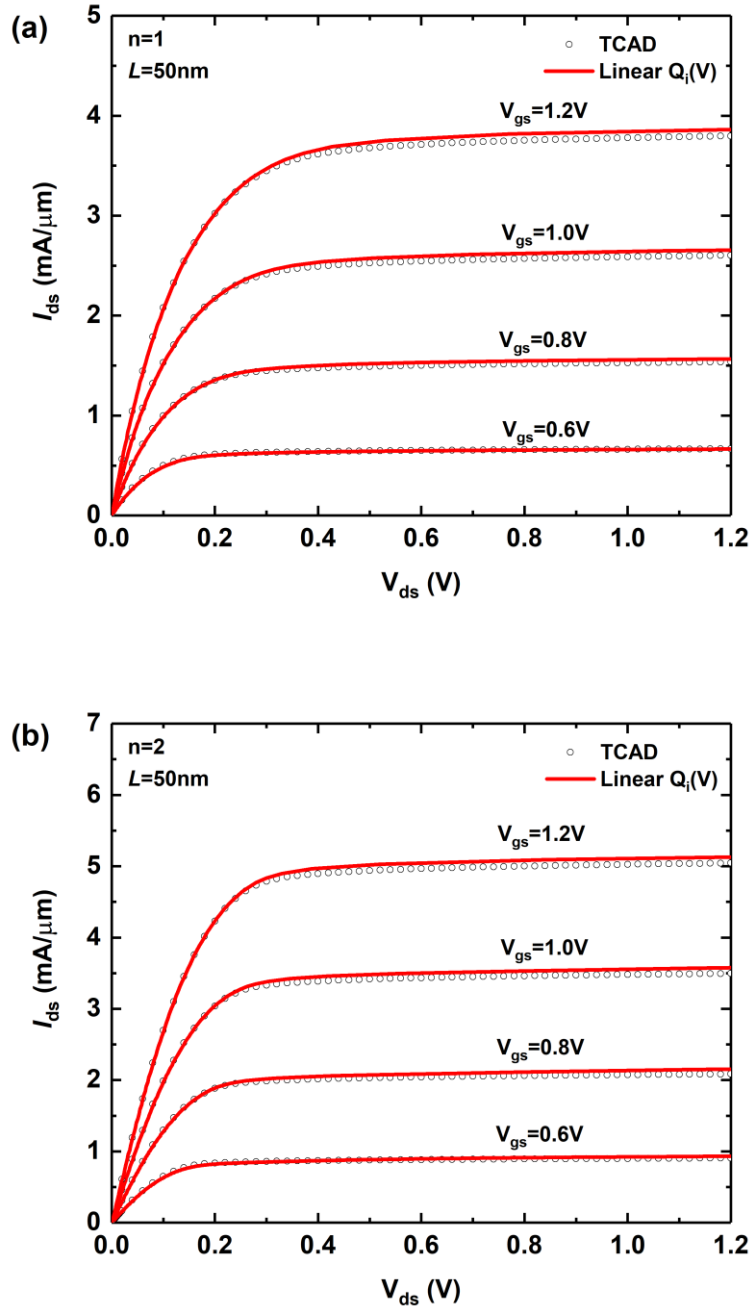


Figure 2 I_{ds} - V_{ds} characteristics for above threshold region generated by linear $Q_i(V)$ model [Eq. (3)] compared with TCAD for (a) $n = 1$ and (b) $n = 2$ velocity saturation cases. $\mu_0=200\text{cm}^2/\text{V}\cdot\text{s}$ and $v_{\text{sat}} = 10^7\text{cm/s}$

in excellent agreement to that of TCAD in above threshold region, illustrating

the effectiveness of including the non-GCA part in the velocity saturation modeling of DG MOSFETs.

Acknowledgement

Part of the data and graphs in this chapter is a reprint of the material as it is in Solid-State Electronics, vol. 166, Art. no. 107766, Ren, Zhongjie, Taur, Yuan. The thesis author was the primary investigator and author of this paper.

Chapter 2: Limitations of Linear $Q_i(V)$ Model in the Near Threshold Region

Although Non-GCA A can successfully generate desirable I-V characteristics in the above threshold region, it is not ideal to facilitate this model in the near threshold region. According to Figs. 3(a) and 3(b), a relative large gap is formed between Non-GCA model with linear $Q_i(V)$ and TCAD data for both $n=1$ and $n=2$ velocity saturation models when we approach into the near threshold region.

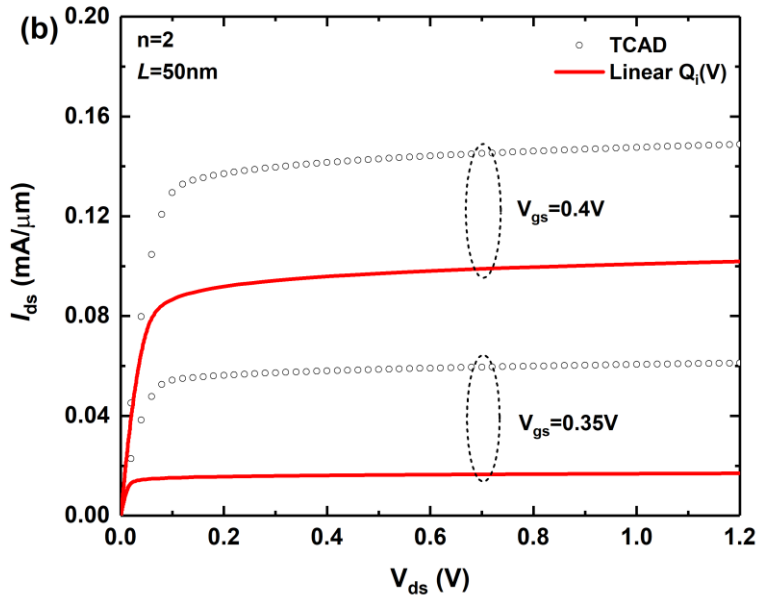
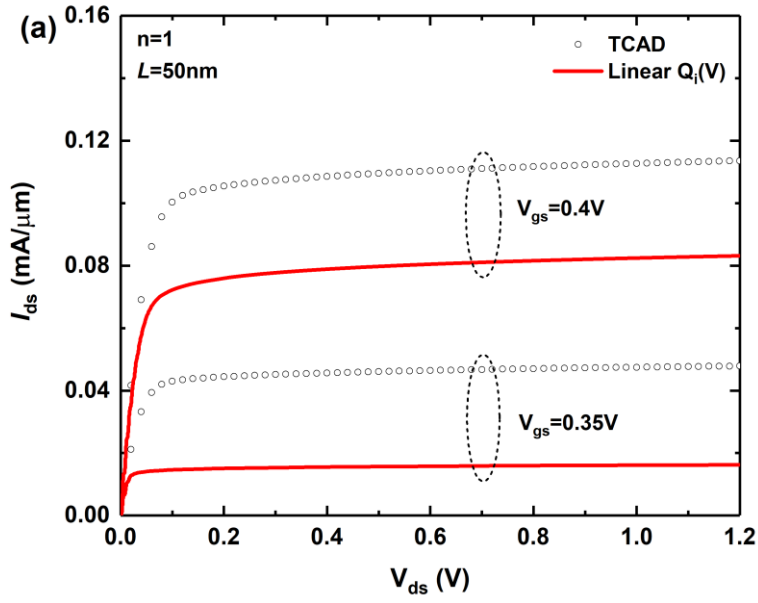


Figure 3 I_{ds} - V_{ds} characteristics for near threshold region generated by Non-GCA model with linear $Q_i(V)$ [Eq.(3)] compared with TCAD for (a) $n = 1$ and (b) $n = 2$ velocity saturation cases

Apparently, Non-GCA model with linear $Q_i(V)$ is no longer suitable for near

threshold modeling in the velocity saturation region since the underestimated I_{ds} generated by this model for $V_{gs}=0.35/0.4V$. In the linear $Q_i(V)$, which is determined by the simplest function under GCA [Eq. (3)], is not accurate enough when V_{gs} is near V_t . According to $Q_i(V)$ plot in Fig. 4(a), Q_i in the linear model is consistent with that calculated by TCAD for the above threshold gate bias and accurately describes where Q_i turns negative. However, as exhibited in Fig. 4(b), considerable separation is observed among the Q_i profiles which are extracted from linear $Q_i(V)$ model and TCAD in the near threshold situation which no longer presents a linear behavior versus the quasi-Fermi level inside the channel, indicating the necessity of utilizing a new model to describe the inversion charge density in this region. It is obvious that the linear $Q_i(V)$ model turns negative earlier than the TCAD data, thereby providing a lower I_{ds} value than the simulation results.

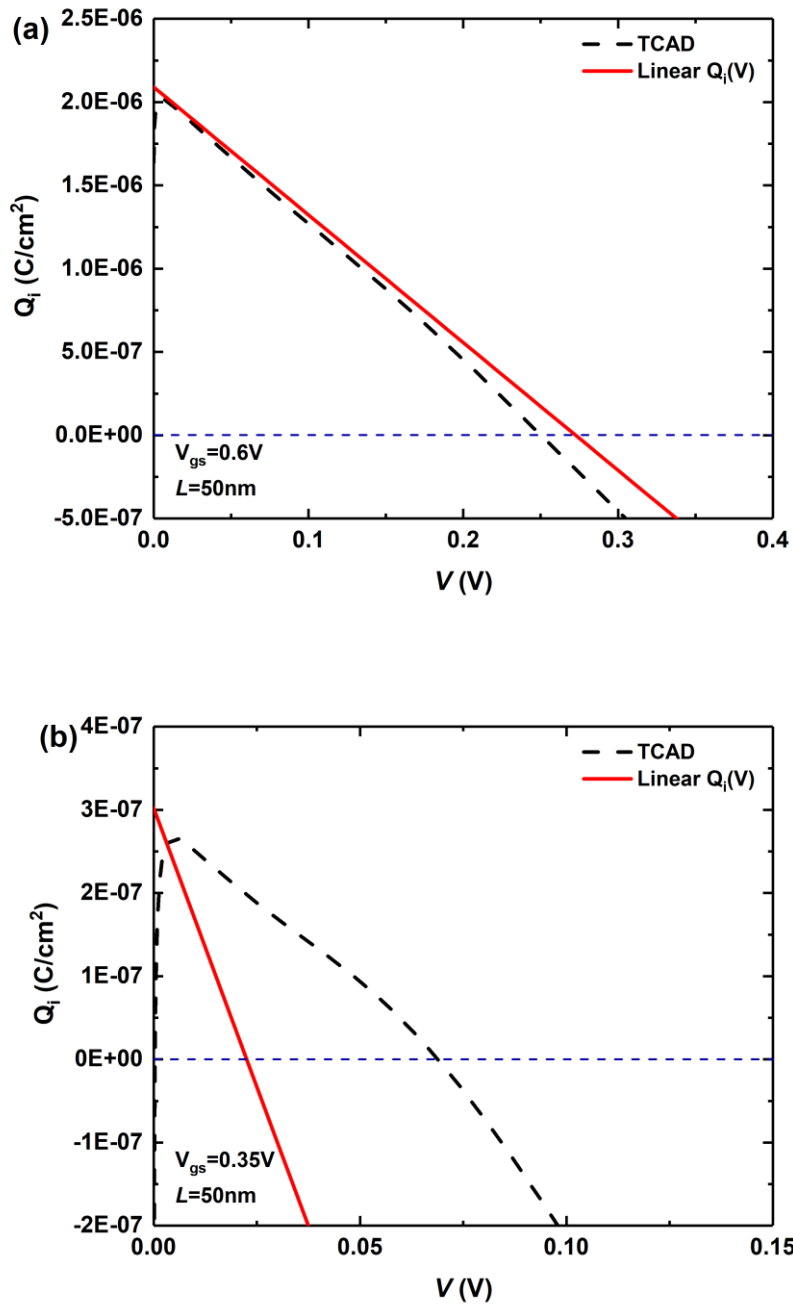


Figure 4 Comparison of $Q_i(V)$ extracted from TCAD and linear model [Eq.(3)] for (a) $V_{gs}=0.6\text{V}$ (above threshold region), (b) $V_{gs}=0.35\text{V}$ (near threshold region)

Acknowledgement

Part of the data and graphs in this chapter is a reprint of the material as it is in Solid-State Electronics, vol. 166, Art. no. 107766, Ren, Zhongjie, Taur, Yuan. The thesis author was the primary investigator and author of this paper.

Chapter 3: Construction of Piecewise $Q_i(V)$ Model

In the undoped DG MOSFET involved in this work, only mobile charges are taken into account thus the Poisson's equation turns to the following form

$$\frac{d^2\psi}{dx^2} + \frac{d^2\psi}{dy^2} = \frac{q}{\epsilon_{si}} n_i e^{q(\psi-V)/kT} \quad (8)$$

where ψ is the potential and n_i is the intrinsic carrier concentration of Silicon. By assuming $d^2\psi/dy^2 \ll d^2\psi/dx^2$, a modified equation is obtained with the removal of the lateral gradient in Eq. (8). Consequently, a continuous model of Q_i can be generated by solving the modified 1-D Poisson's equation [2]:

$$Q_i = 8 \frac{kT}{q} \frac{\epsilon_{si}}{t_{si}} \beta \tan \beta \quad (9)$$

where β is a constant which is independent of x , the relation between β and V inside the device is established by

$$V_{gs} - V_t - V = \frac{2kT}{q} \left[\ln \beta - \ln(\cos \beta) + 2 \frac{\epsilon_{si} t_i}{\epsilon_i t_{si}} \beta \tan \beta \right] \quad (10)$$

With

$$V_t \equiv \phi_m - \chi - \frac{E_g}{2q} + \frac{2kT}{q} \ln \sqrt{\frac{8\epsilon_{si}kT}{q^2 n_i t_{si}^2}} \quad (11)$$

In the equations above, ϕ_m is the gate work function and χ is the electron affinity of Silicon. This continuous Q_i model is more rigorous than the simplest approximation used in Eq. (3) but it can not go negative since LHS of Eq. (8) is always positive which restricts its application to long channel MOSFETs ($L \sim 1\mu\text{m}$). Additionally, the $Q_i(V)$ model from eq.(8) could fit the nonlinear behavior of TCAD results in the near-source side of the channel, as shown in Fig. 5. In order to combine it with non-GCA part, Q_i in Eq.(8) should be artificially adjusted by adding an additional term which will make it go negative around $V=V_{gs}-V_t$ in a recent constant mobility model [9]. However, it is clear that this assumption no longer works for near threshold region due to the mismatch of Non-GCA with linear $Q_i(V)$ and TCAD data, demonstrating a switch of zero point and a piecewise behavior in TCAD data under the near threshold gate bias.

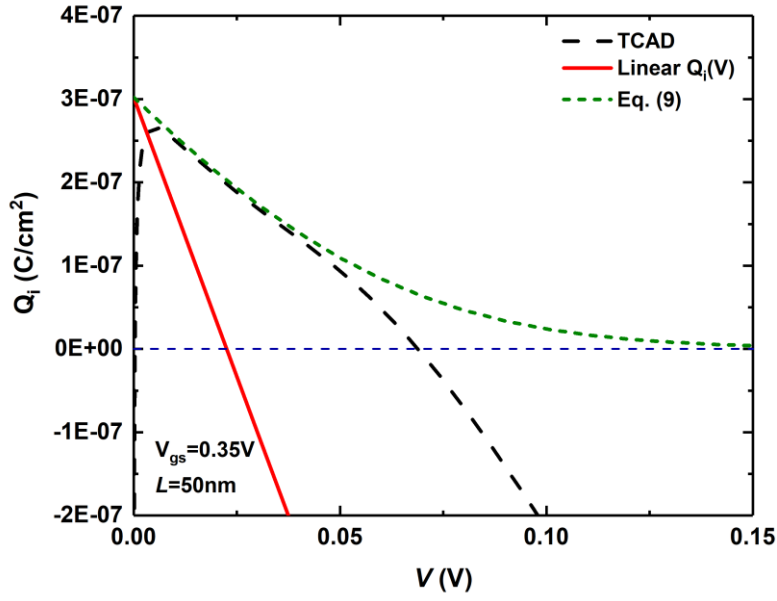


Figure 5 Comparison of $Q_i(V)$ extracted from TCAD , linear model [Eq.(3)] and Eq. (9) for $V_{gs}=0.35V$ (near threshold region)

In order to modify Eq. (9) to create a new nonlinear $Q_i(V)$ function, a turning point must be found to approach the TCAD behavior. The tangent of Eq. (9) at the source side (defined as $G(V)$) might be a good method to solve the turning point. By take the derivatives of Q_i and V with respect to β , we can obtain the following relations at the source

$$\left. \frac{dQ_i}{d\beta} \right|_{V=0} = 8 \frac{kT}{q} \frac{\epsilon_{si}}{t_{si}} (\tan \beta_s + \beta_s \sec^2 \beta_s) \quad (12)$$

$$\left. \frac{dV}{d\beta} \right|_{V=0} = -\frac{2kT}{q} \left[\frac{1}{\beta_s} + \tan \beta_s + 2 \frac{\epsilon_{si} t_i}{\epsilon_i t_{si}} (\tan \beta_s + \beta_s \sec^2 \beta_s) \right] \quad (13)$$

where β_s is $\beta(V=0)$ solved from Eq. (10). It is strightforward to figure out the slope of $G(V)$ by combining Eq. (12) with Eq. (13)

$$\left. \frac{dQ_i}{dV} \right|_{V=0} = 4 \frac{\varepsilon_{si}}{t_{si}} \frac{\tan \beta_s + \beta_s \sec^2 \beta_s}{\frac{1}{\beta_s} + \tan \beta_s + 2 \frac{\varepsilon_{si} t_i}{\varepsilon_i t_{si}} (\tan \beta_s + \beta_s \sec^2 \beta_s)} \quad (14)$$

Thus, $G(V)$ is given by

$$G(V) = Q_i(V=0) \left(1 - \frac{mV}{V_{gs} - V_t} \right) \quad (15)$$

And the turning point:

$$V(G=0) = \frac{V_{gs} - V_t}{m} \quad (16)$$

with

$$\begin{aligned} m &= - \frac{V_{gs} - V}{Q_i(V=0)} \left. \frac{dQ_i}{dV} \right|_{V=0} \\ &= \frac{\left(\frac{1}{\beta_s} + \tan \beta_s + \frac{1}{\tan \beta_s} \right) \times \left(\ln \beta_s - \ln(\cos \beta_s) + 2 \frac{\varepsilon_{si} t_i}{\varepsilon_i t_{si}} \beta_s \tan \beta_s \right)}{\frac{1}{\beta_s} + \tan \beta_s + 2 \frac{\varepsilon_{si} t_i}{\varepsilon_i t_{si}} (\tan \beta_s + \beta_s \sec^2 \beta_s)} \quad (17) \end{aligned}$$

Clearly, the $Q_i(V)$ in TCAD will form a nonlinear behavior for near threshold region. The plot of $G(V)$, although can not fully reproduce Q_i profile, can precisely predict the turning point for $Q_i(V)$ which will pave the way for introduction of the accurate piecewise $Q_i(V)$ model, as illustrated in Fig. 6.

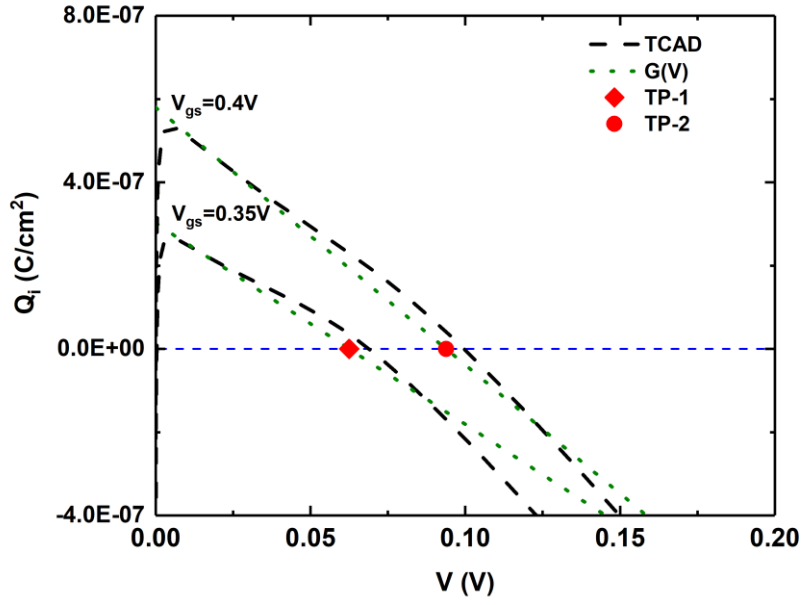


Figure 6 Comparison of $Q_i(V)$ extracted from TCAD and turning points (TP-1 & TP-2) for $V_{gs}=0.35/0.4V$ calculated by facilitating $G(V)$

Considering the continuity of new nonlinear $Q_i(V)$ model, a straightforward idea of making $Q_i(V)$ symmetric based on Eq. (9) by defining the center of symmetry at $(V_{gs}-V_t/m, Q_{TP}=Q_i(V=V_{gs}-V_t/m))$ and thus get a piecewise function of $Q_i(V)$ given by

$$Q_i = \begin{cases} 8 \frac{kT}{q} \frac{\epsilon_{si}}{t_{si}} \beta \tan \beta, V \leq \frac{V_{gs} - V_t}{m} \\ 2Q_{TP} - 8 \frac{kT}{q} \frac{\epsilon_{si}}{t_{si}} \beta' \tan \beta', V > \frac{V_{gs} - V_t}{m} \end{cases} \quad (18)$$

With β' solved by

$$V + \left(\frac{m-2}{m} \right) (V_{gs} - V_t) = \frac{2kT}{q} \left[\ln \beta' - \ln (\cos \beta') + 2 \frac{\epsilon_{si} t_i}{\epsilon_i' t_{si}} \beta' \tan \beta' \right] \quad (19)$$

However, although it can successfully extend the $Q_i(V)$ to go negative, this Eq.(18) can not successfully fit the TCAD data since the $Q_i(V)$ from TCAD is

not centrosymmetric at near threshold region (Fig. 7). Therefore, a modified piecewise model is generated by scaling the $V > V_{gs} - V_t/m$ part of Eq. (18) in both x and y directions to obtain a steeper slope which is consistent with TCAD data (Fig. 9) and thereby changing Eq. (18) to

$$Q_i = \begin{cases} 8 \frac{kT}{q} \frac{\epsilon_{si}}{t_{si}} \beta \tan \beta, V \leq \frac{V_{gs} - V_t}{m} \\ \frac{3}{2} Q_{TP} - 4 \frac{kT}{q} \frac{\epsilon_{si}}{t_{si}} \beta'' \tan \beta'', V > \frac{V_{gs} - V_t}{m} \end{cases} \quad (20)$$

With β'' solved by

$$V + \left(\frac{m-3}{m} \right) (V_{gs} - V_t) = \frac{2kT}{q} \left[\ln \beta'' - \ln (\cos \beta'') + 2 \frac{\epsilon_{si} t_i}{\epsilon_i t_{si}} \beta'' \tan \beta'' \right] \quad (21)$$

Velocity saturation models facilitating Eq. (20) as the function of $Q_i(V)$ are defined as the proposed Non-GCA model in this work. Consequently, this Non-GCA model with piecewise $Q_i(V)$ can excellently reproduce the piecewise behavior in $Q_i(V)$ profiles of the near threshold region which is not accessible for conventional Non-GCA model and thereby making it possible to fill the blank in the velocity saturation modeling of this region.

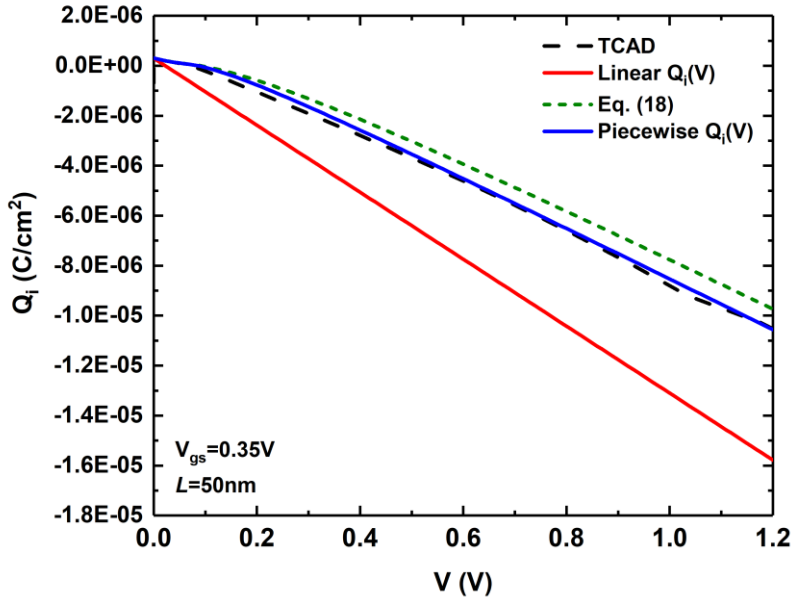


Figure 7 Comparison of $Q_i(V)$ extracted from TCAD, linear model [Eq.(3)] , Eq. (19) and piecewise model [Eqs.(20) and (21)] for $V_{gs}=0.35V$

Acknowledgement

Part of the data and graphs in this chapter is a reprint of the material as it is in Solid-State Electronics, vol. 166, Art. no. 107766, Ren, Zhongjie, Taur, Yuan.

The thesis author was the primary investigator and author of this paper.

Chapter 4: Non-GCA Model with Piecewise $Q_i(V)$ for the Near-Threshold Region

The $Q_i(y)$ and $V(y)$ profiles extracted through the integration process of the Non-GCA modeling, which are mainly decided by the $Q_i(V)$ model, are closely

related to the corresponding I-V characteristics calculated by the model. Those $Q_i(y)$ and $V(y)$ profiles based on the linear $Q_i(V)$ shows a considerable separation from the TCAD data. In contrast, thanks to the modified piecewise $Q_i(V)$ function, the $Q_i(y)$ and $V(y)$ profiles calculated from it present a consistent behavior with the results of TCAD simulations, as shown in Figs. 8 and 9. The comparison of $Q_i(y)$ and $V(y)$ in Figs. 8 and 9 is based on $n = 1$ model and similar results could be testified for $n = 2$ model as well.

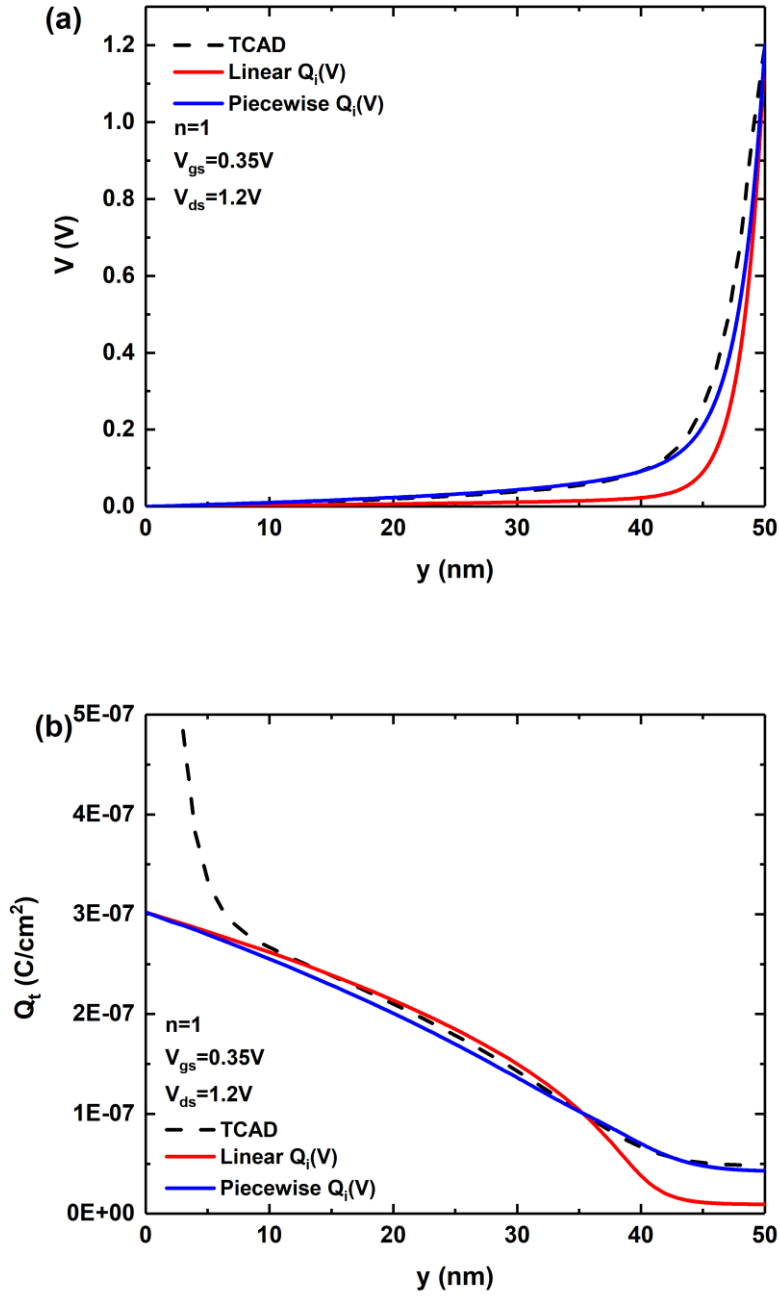


Figure 8 (a) $V(y)$ and (b) $Q_t(y)$ in the channel extracted from TCAD, non-GCA model with linear $Q_i(V)$ [Eq.(3)] and piecewise $Q_i(V)$ [Eqs.(20) and (21)] for $V_{gs}=0.35V$ and $V_{ds}=1.2V$

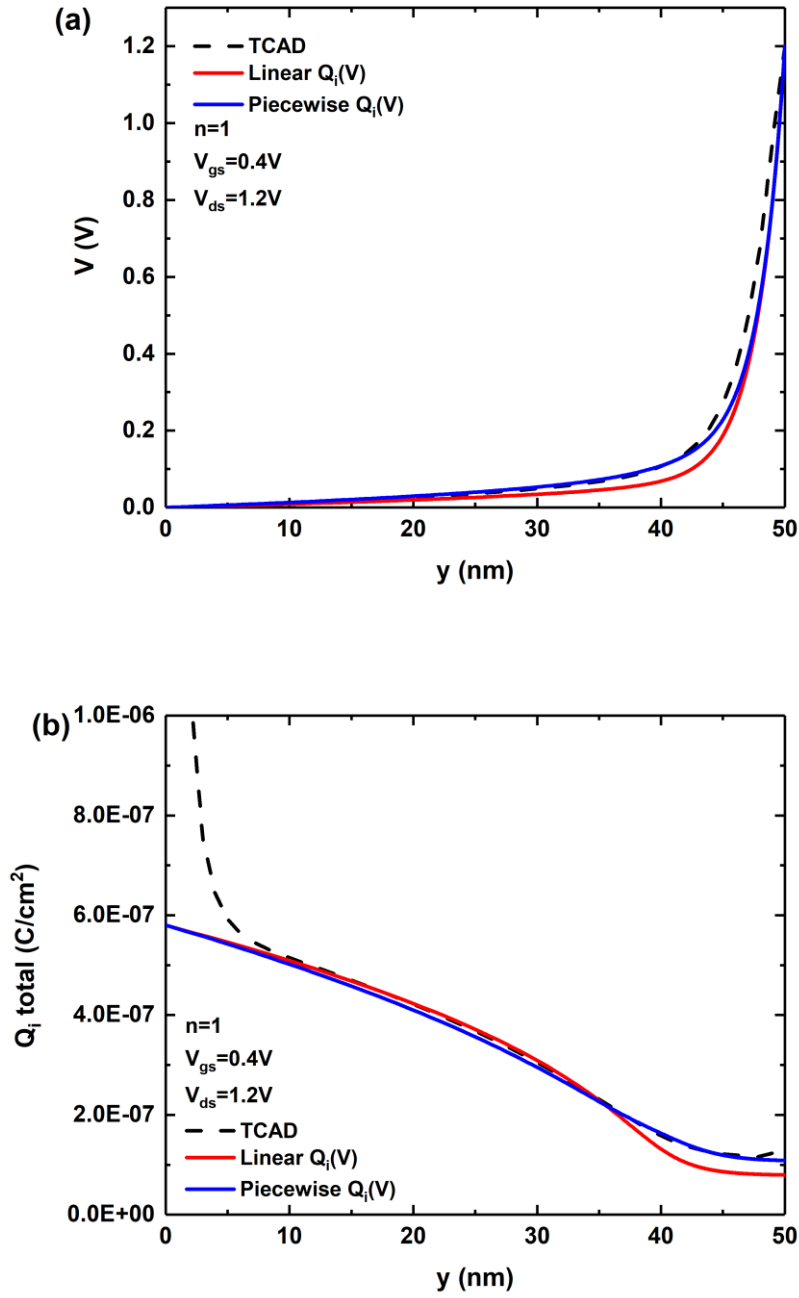


Figure 9 (a) $V(y)$ and (b) $Q_i(y)$ in the channel extracted from TCAD, non-GCA model with linear $Q_i(V)$ [Eq.(3)] and piecewise $Q_i(V)$ [Eqs.(20) and (21)] for $V_{gs}=0.4V$ and $V_{ds}=1.2V$

The V value at $y=50\text{nm}$ is the same as the V_{ds} of the device. Evidently, in the near-source side of the device, linear $Q_i(V)$ model could obtain a similar $Q_t(V)$ value with TCAD data (except the source encroachment part) while providing a smoother slope of $V(y)$ than simulation results. According to the Eq. (1) and (2), it should reflect a smaller I_{ds} value than that of TCAD. Analogously, the smaller $Q_t(V)$ and relatively good dV/dy approximation calculated from linear $Q_i(V)$ model in comparison to TCAD in the near-drain side of the device indicates a smaller I_{ds} value as well. Those behaviors of linear $Q_i(V)$ model have been successfully revised by the introduction of piecewise $Q_i(V)$ model. Accordingly, a significantly improved I-V modeling could be calculated from the proposed model in the near-threshold region, as illustrated in Fig. 10.

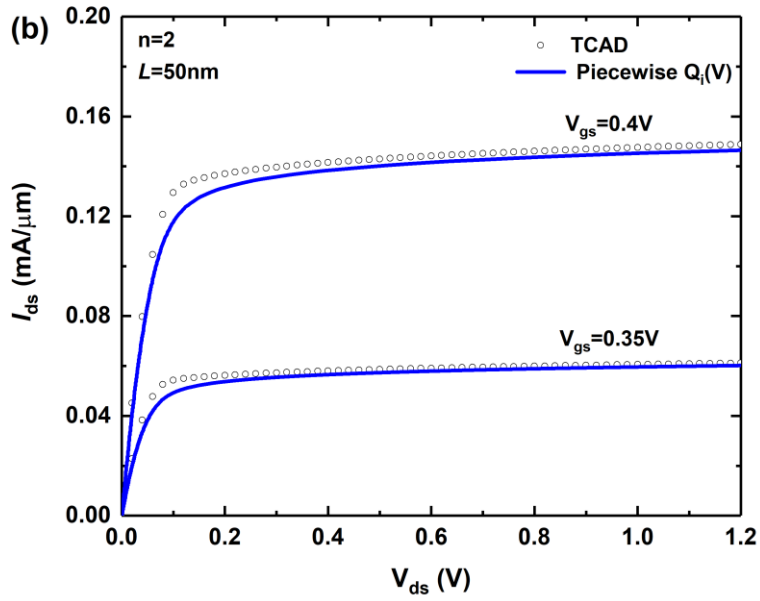
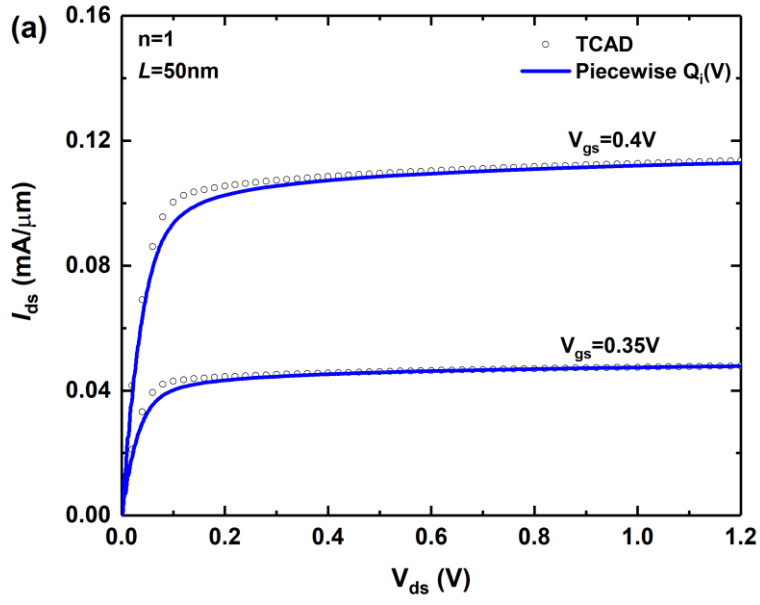


Figure 10 I_{ds} - V_{ds} characteristics ($n = 1$ velocity saturation case) for the near threshold region generated by non-GCA model with piecewise $Q_i(V)$ [Eqs.(20) and (21)] compared with TCAD for (a) $n = 1$ and (b) $n = 2$ velocity saturation cases.

There is a slight discrepancy (5-10%) of the modeled curves with TCAD in the region approaching saturation in both Fig. 10(a) and Fig. 10(b). This is due to source-drain encroachment (a.k.a. carrier spillover) shown in Fig. 11 where the total mobile charge density Q_t is plotted between the source and drain. The encroachment length is ~ 5 nm from TCAD, generally in line with the error figure mentioned above for an $L = 50$ nm device.

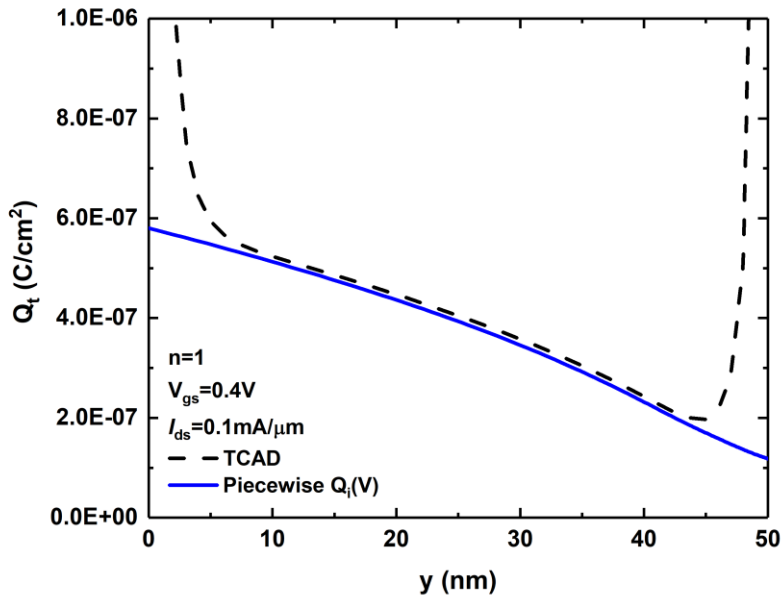


Figure 11 Comparison of $Q_t(y)$ in the channel between the non-GCA model with piecewise $Q_i(V)$ [Eqs.(20) and (21)] and TCAD.

Figure 12 compares the I_{ds} - V_{gs} curves generated from this model with piecewise $Q_i(V)$ to TCAD simulations for a fixed V_{ds} of 1.2 V. Also shown are those generated from the model with linear $Q_i(V)$ [3]. The contrast is clear. While both models are accurate for V_{gs} at least 0.2 V (~ 10 kT/q) above V_t (~ 0.33 V), only the model with piecewise $Q_i(V)$ is accurate in the near-threshold

region. Furthermore, the accurate I_{ds} - V_{ds} characteristics could be generated by the non-GCA model with piecewise $Q_i(V)$ in the above threshold region for both $n = 1$ and $n = 2$ velocity saturation cases, as shown in Fig. 13.

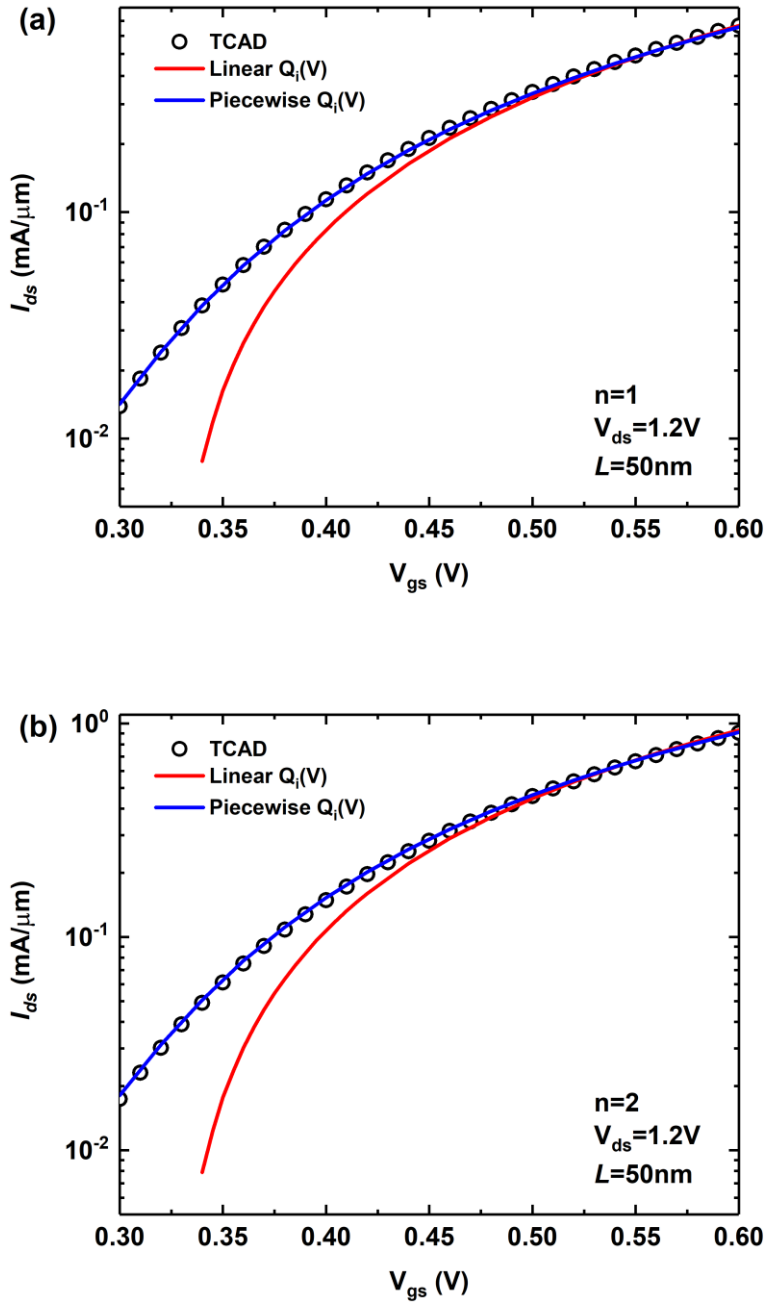


Figure 12 I_{ds} - V_{gs} characteristics generated by the non-GCA model with linear $Q_i(V)$ [Eq. (2)] and with piecewise $Q_i(V)$ [Eqs.(20) and (21)] compared to

TCAD for (a) $n = 1$ and (b) $n = 2$ velocity saturation models. $V_t \sim 0.33$ V in this case.

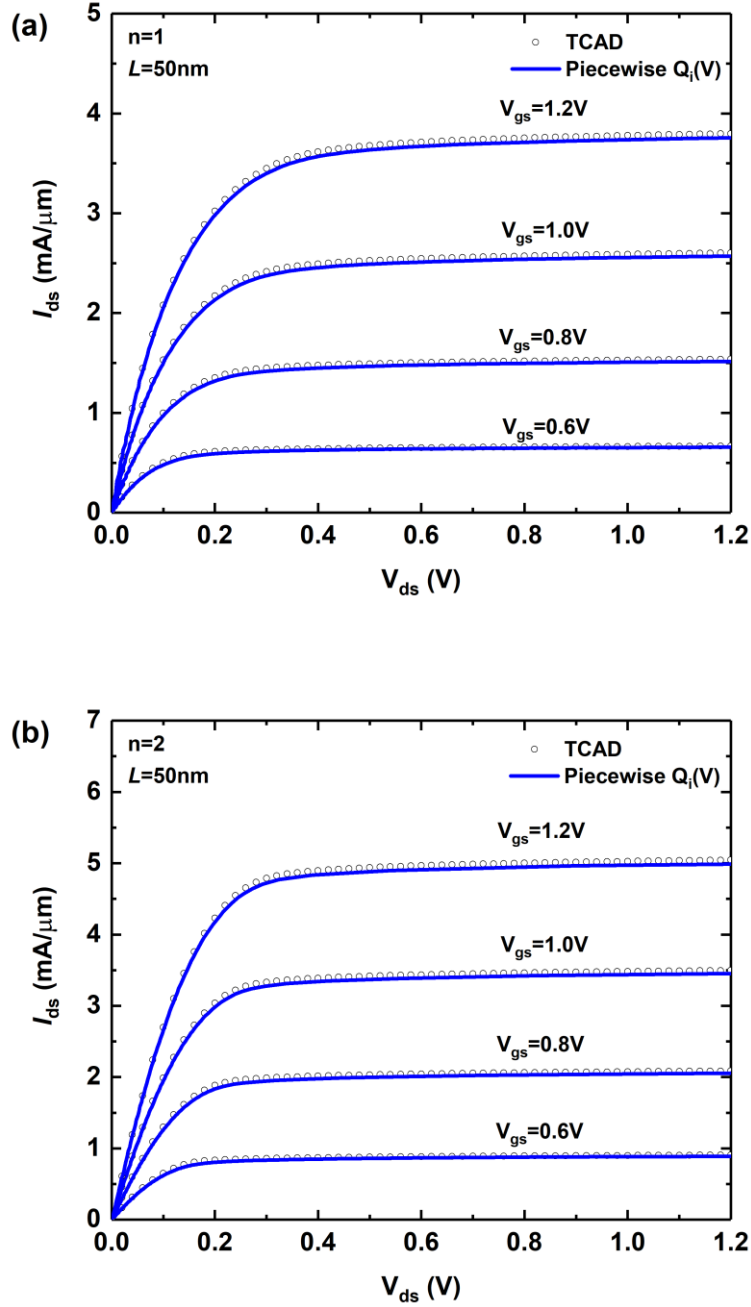


Figure 13 I_{ds} - V_{ds} characteristics for the above threshold region generated by non-GCA model with piecewise $Q_i(V)$ [Eqs.(20) and (21)] compared with TCAD for (a) $n = 1$ and (b) $n = 2$ velocity saturation cases.

Acknowledgement

Part of the data and graphs in this chapter is a reprint of the material as it is in Solid-State Electronics, vol. 166, Art. no. 107766, Ren, Zhongjie, Taur, Yuan. The thesis author was the primary investigator and author of this paper.

Conclusion

In this work, it is shown that the non-GCA model with linear $Q_i(V)$ fails to model the near threshold region properly. Although it works well in the above threshold region, the nonlinear $Q_i(V)$ behavior near the threshold could not be described by this model. The all-region GCA could model the nonlinear $Q_i(V)$ of 2D simulations before it goes negative. Therefore, a new piecewise $Q_i(V)$ model is constructed by stitching an inverted portion of the $Q_i(V)$ curve from this all-region GCA model onto itself. It satisfies the non-GCA requirement that $Q_i(V)$ goes negative when the vertical gate field changes sign near the drain. This $Q_i(V)$ model is shown to produce $I_{ds}-V_{ds}$ characteristics consistent with TCAD in the near threshold as well as beyond threshold regions for both $n = 1$ and $n = 2$ velocity saturation models.

References

- [1] Y. Taur, "An analytical solution to a double-gate MOSFET with undoped body," *IEEE Electron Device Lett.*, vol. 21, no. 5, pp. 245-247, May 2000.
- [2] Y. Taur, X. Liang, W. Wang and H. Lu, "A continuous, analytic drain-current model for DG MOSFETs," *IEEE Electron Device Lett.*, vol. 25, no. 22, pp.107-109, Feb. 2004.
- [3] H. Lu and Y. Taur, "An analytic potential model for symmetric and asymmetric DG MOSFETs," *IEEE Trans. Electron Devices*, vol. 53, no. 5, pp.1161-1168, May 2006.
- [4] F. Lime, E. Santana and B. Iñiguez, "A simple compact model for long-channel junctionless Double Gate MOSFETs," *Solid-State Electronics*, vol. 80, pp. 28-32, Feb. 2013.
- [5] Y. Taur and T. H. Ning, *Fundamentals of Modern VLSI Devices*, Cambridge, U.K.: Cambridge Univ. Press, 2013.
- [6] Y. Taur, W. Choi, J. Zhang and M. Su, "A Non-GCA DG MOSFET Model Continuous into the Velocity Saturation Region," *IEEE Trans. Electron Devices*, vol. 66, no. 3, pp.1160-1166, Mar. 2019.
- [7] *ATLAS Device Simulation Software User's Manual*, Silvaco, Inc., Santa Clara, CA, USA, 2015.
- [8] V. Hariharan, J. Vasi and V. R. Rao, "Drain Current Model Including Velocity Saturation for Symmetric Double-Gate MOSFETs," *IEEE Trans. Electron Devices*, vol. 55, no. 8, pp. 2173-2180, Aug. 2008.
- [9] Y. Taur and H.-H. Lin, "Modeling of DG MOSFET I-V Characteristics in the Saturation Region," *IEEE Trans. Electron Devices*, vol. 65, no. 5, pp. 1714-1720, May 2018.